arXiv:cond-mat/0301186v1 [cond-mat.mtrl-sci] 13 Jan 2003

Free boundary problems describing two-dimensional pulse recycling and motion in semiconductors

L. L. Bonilla [*]

Departamento de Matemáticas, Universidad Carlos III de Madrid,

Avda. Universidad 30, E-28911 Leganés, Spain

Also: Unidad Asociada al Instituto de Ciencia

de Materiales (CSIC), 28049 Cantoblanco, Spain

R. Escobedo[†]

MIRIAM (MIlan Research center for Industrial and Applied Mathematics)

Dipartimento di Matematica, Università di Milano,

Via Saldini 50; 20133 Milano, Italy

F. J. Higuera[‡]

ETS Ingenieros Aeronáuticos, Universidad Politécnica de Madrid,

Pza. Cardenal Cisneros 3, 28040 Madrid, Spain.

(Dated: February 2, 2008)

Abstract

An asymptotic analysis of the Gunn effect in two-dimensional samples of bulk n-GaAs with circular contacts is presented. A moving pulse far from contacts is approximated by a moving free boundary separating regions where the electric potential solves a Laplace equation with subsidiary boundary conditions. The dynamical condition for the motion of the free boundary is a Hamilton-Jacobi equation. We obtain the exact solution of the free boundary problem (FBP) in simple one-dimensional and axisymmetric geometries. The solution of the FBP is obtained numerically in the general case and compared with the numerical solution of the full system of equations. The agreement is excellent so that the FBP can be adopted as the basis for an asymptotic study of the multi-dimensional Gunn effect.

PACS numbers: 73.50.Fq, 73.61.Ey

I. INTRODUCTION

Excitable media exhibit a large response to a sufficiently strong disturbance from their only stable stationary homogeneous state. This feature makes them ideally suited to sustain propagation of pulses or wave trains [1]. Examples are the propagation of an action potential along the axon of a nerve [2], the propagation of a grass fire on a prairie, pulse propagation through cardiac cells [2], reaction-diffusion [3] or ecological systems [1]. Semiconductor systems displaying negative differential resistivity in their current-field characteristics are also excitable systems albeit they have peculiar features due to the long range character of the electromagnetic interaction [4]. Thus *dc* voltage bias conditions lead to pulse recycling (at contacts) and motion that give rise to self-sustained oscillations of the electric current, the so-called Gunn effect, [5]. While most of the theoretical and experimental studies of these phenomena deal with one dimensional geometries of samples with attached planar contacts, recent experiments [6] and numerical studies [7, 8] have considered rectangular samples with point contacts. In this case, many unusual oscillatory patterns are found [7, 8].

A large part of the literature on pulse propagation is devoted to the mathematical description of their motion on one-dimensional unbounded domains. In the case of self-oscillations in semiconductor systems, such a description is the basis of asymptotic analyses of pulse recycling and motion, both in one-dimensional (1D) [9, 10] or axisymmetric two-dimensional (2D) samples [7, 11]. These studies exploit that the electric field has only one relevant component whose integral yields the voltage difference between contacts. The situation is very different in more general geometries and new ideas need to be brought in. In this paper, we reduce pulse propagation (far from contacts) to the motion of a free boundary (FB) separating regions where the electric potential is a harmonic function. The FB obeys a Hamilton-Jacobi equation (HJE). On the FB, continuity and jump conditions hold, and additional conditions on contacts and sample boundaries are needed for the problem of finding the FB (free boundary problem or FBP) to have a unique solution. On simple 1D and axisymmetric geometries, the HJE can be solved exacly. Its solution describes very well the motion of a discontinuity of the electric potential representing the pulse far from the boundaries, as comparison with the numerical solution of the full system of differential equations shows. This is also true of the general 2D case, but now the solution of the FBP has to be obtained numerically. In all cases, recycling and annihilation of pulses at contacts have to

be described separately from the FB motion.

The rest of the paper is organized as follows. In Section II, we present the governing equations of the Kroemer model for the Gunn effect in two-dimensional samples of n-GaAs. An asymptotic derivation of the FBP is given in Section III. Section IV contains the exact solutions of the FBP in the 1D and axisymmetric cases. Numerical solutions of the FBP in the general 2D case and comparisons with the numerical solution of the full system of equations are presented in Section V. The last Section contains our conclusions.

II. EQUATIONS AND BOUNDARY CONDITIONS

The Kroemer model [12] consists of the following equations and boundary conditions (in dimensionless units) for the concentration of free carriers (electrons), n, and the electric potential, φ:

$$\frac{\partial n}{\partial t} + \vec{\nabla} \cdot (n\vec{v} - \delta\vec{\nabla} n) = 0, \tag{1}$$

$$\vec{\nabla}^2 \varphi = n - 1, \tag{2}$$

$$\vec{v}(\vec{E}) = \vec{E}\,\frac{1 + v_s E^3}{1 + E^4}\,, \tag{3}$$

$$\vec{x} \in \Sigma_c: \quad \vec{E}\cdot\vec{N} = \rho\,(n\vec{v} - \delta\vec{\nabla} n)\cdot\vec{N} \quad \text{and} \quad \varphi = 0, \tag{4}$$

$$\vec{x} \in \Sigma_a: \quad \vec{E}\cdot\vec{N} = \rho\,(n\vec{v} - \delta\vec{\nabla} n)\cdot\vec{N} \quad \text{and} \quad \varphi = \Phi, \tag{5}$$

$$\vec{x} \in \Sigma_o: \quad \vec{E}\cdot\vec{N} = 0 \quad \text{and} \quad (n\vec{v} - \delta\vec{\nabla} n)\cdot\vec{N} = 0. \tag{6}$$

Here (1) and (2) are the charge continuity and Poisson equations, respectively. The dimensionless electric field is $\vec{E} = \vec{\nabla}\varphi$ and $E = |\vec{E}|$. In these equations, the electron density has been scaled with the uniform concentration of donor impurities in the semiconductor, $N_D = 10^{15}$ cm^{-3}, and the electric field with the field characterizing the intervalley transfer responsible for the negative differential mobility involved in the Gunn oscillation, $E_R = 3.1$ kV/cm. Distances and times have been measured with the dielectric length and the dielectric relaxation time, $l_1 = \epsilon E_R/(eN_D) \approx 0.276\mu$m, $l_1/(\mu_0 E_R) \approx 1.02$ ps, respectively (μ_0 is the zero-field electron mobility; see, *e.g.*, [9] for details). The unit of electric potential is $E_R l_1 \approx 0.011$ V. The carrier drift velocity of Eq. (3), $\vec{v}(\vec{E})$, is already written in dimensionless units, and it has been depicted in Fig. 1 of Ref. 7. We assume that the diffusion coefficient is constant, $\delta \approx 0.013$ (at 20K). In the rest of the paper we assume also a zero saturation velocity: $v_s = 0$.

Boundary and bias conditions need to be imposed at the interfaces between semiconductor and contacts, $\Sigma_{c,a}$, and on the outer boundary of the semiconductor boundary Σ_o. Our boundary conditions (4) and (5) assume that the normal components of electron current density and electric field are proportional at the semiconductor–contact boundary (Ohm's law) [9], (in these equations, $\vec{N}$ is the unit normal to $\Sigma_{c,a}$, directed towards the semiconductor). For simplicity, we choose all contact resistivities ρ to be equal. Bias conditions are chosen to be $\varphi = 0$ at the cathode Σ_c (injecting contact) and $\varphi = \Phi$ (the applied voltage) at the anode Σ_a (receiving contact). If part of the semiconductor boundary does not have attached contacts, the corresponding boundary conditions are zero flux ones, as in Eq. (6). Typically $\delta > 0$ is very small, so that diffusion matters only inside boundary layers near the contacts or inside thin shock waves [9, 10]. The latter are charge accumulations that will be treated simply as discontinuities of the electric field [9]. Thus diffusion effects may be left out of the conservation equation (1) when interpreting the results. If we set $\delta = 0$, the first boundary condition in Eq. (5) and the second one in Eq. (6) should be omitted.

We can write an Ampère's equation for the total current density (electronic plus displacement), $\vec{j}$, by eliminating n from (1) using (2):

$$\vec{\nabla} \cdot \vec{j} = 0, \qquad \text{with}$$
$$\vec{j} = (1 + \vec{\nabla}^2\varphi)\vec{v} - \delta\,\vec{\nabla}(\vec{\nabla}^2\varphi) + \frac{\partial \vec{E}}{\partial t}\,. \tag{7}$$

III. DERIVATION OF THE FREE BOUNDARY PROBLEM

Let us consider a rectangular sample with circular contacts whose radii r_c are large but much smaller than the distance between contacts, $1 \le r_c \ll L$. The current density varies slowly and follows adiabatically the electric field profiles in the semiconductor except during brief periods in which new pulses are shed from the cathodes. Close to a cathode located at the origin, the electric field and the current density are approximately axisymmetric and we can use the results of Ref. 11. $\vec{j} = J\vec{r}/r^2$, $r = |\vec{r}|$, $\vec{E} = E_1(J/r)\vec{r}/r$. $E_1(j)$ and $E_2(j)$, with $E_1 < E_2$, are the two positive zeros of the function $v(E) - j$, with $v(E) = |\vec{v}(\vec{E})|$. The maximum value of $|\vec{j}|$ during self-oscillations is somewhat larger than $j_c = O(1)$ at which $E_2(j) = \rho j$. Correspondingly, the maximum value of J is $J_c = j_c r_c = O(r_c)$ and far from the cathode, $r \gg r_c$, $J \ll r$ holds. This means that $E \sim E_1(J/r) \approx J/r \ll 1$ and $v(E) \approx E$.

When $v_s = 0$ the pulses move slowly over large regions of the sample in which the field is stationary and small: $E \ll 1$. Notice that $v(E) = E - E^5/(1+E^4)$, which implies $v(E)$ to be approximately linear on a wide range of field values, $E^5 \ll 1$. We conclude that $v(E) \approx E$ except near the contacts and inside pulses. In these outer regions, space and time derivatives can be neglected in Eq. (7), which implies $\vec{j} \approx \vec{v}(\vec{E}) \approx \vec{E}$ there. Thus $\mathrm{div}\vec{j} = 0$ yields $\vec{\nabla}^2\varphi = 0$ and the electric potential φ is a harmonic function outside pulses and contact regions:

$$\vec{\nabla}^2\varphi = 0. \tag{8}$$

Let us now consider the pulse interior. A pulse is a narrow region of high electric field bounded by a leading front and a trailing front which is a shock wave. Outside the pulse $E \ll 1$ as explained before. The leading front is a region at which $n = 1 + \vec{\nabla}\cdot\vec{E} \approx 0$. Since we are describing the pulse far from the contacts, $r \gg r_c \gg 1$, the electric field is essentially normal to the pulse, $\vec{N}$. Then $E_N = \vec{E}\cdot\vec{N} \approx r_w(t) - r$, where r measures displacement along the normal to the front and $r_w(t)$ yields the front location. The velocity of the leading front is $dr_w/dt = j_N = \vec{j}\cdot\vec{N}$, according to Eq. (7). The back of a triangular pulse of height $(E_+ - E_-)$ (the trailing front) is a shock wave with speed given by the equal area rule [11]

$$V(E_+, E_-) = \frac{1}{E_+ - E_-}\int_{E_-}^{E_+} v(E)\,dE \sim \frac{\pi}{4E_+}, \tag{9}$$

where we have used that $E_- \sim E_1$ [13] as $E_+ \gg 1$. Then the trailing front velocity is small and small waves move faster than large ones. A key observation is that the pulse is *narrow* and it can be substituted by a curve on a length scale of the order of the distance between contacts, L. This is clear if leading and trailing fronts of the pulse are circular [11]. Then the bias $\Phi = O(L)$ is the integral of the electric field from the cathode to the anode and the pulse width (equal to its height) is $(E_+ - E_-) = O(\sqrt{\Phi}) \ll \Phi$. In the general case, the pulses are circular during a large part of their lives [7] and we shall assume that their widths remain much smaller than L even when their shapes are no longer circular. Then we assume that the pulses are curves Γ given by the equation:

$$W(\vec{x}, t) = 0. \tag{10}$$

Clearly, there is a finite voltage drop across the pulse, $\sim E_+^2/2 = O(\Phi)$, which means that the electric potential has a jump discontinuity at Γ:

$$\frac{E_+^2}{2} = [\varphi] \equiv \varphi_+ - \varphi_-. \tag{11}$$

Here φ_- and φ_+ are the limiting values of φ as $\vec{x}$ approaches Γ from the region inside or outside Γ, respectively. The relations $\mathrm{div}\vec{j} = 0$ and $\vec{j} \approx \vec{E}$ imply that the normal component of the electric field (and therefore the normal derivative of the electric potential) is continuous across Γ:

$$j_N = (\vec{N} \cdot \vec{\nabla}\varphi)_+ = (\vec{N} \cdot \vec{\nabla}\varphi)_-. \tag{12}$$

This j_N is also the velocity of the leading front of the pulse along its normal, which is nearly equal to that of the trailing front, V given by Eq. (9), during most of the pulse lifetime. The pulse velocity can also be obtained by differentiating Eq. (10) with respect to time:

$$\frac{\partial W}{\partial t} + \vec{\nabla} W \cdot \frac{d\vec{x}}{dt} = 0.$$

Since $\vec{N} = \vec{\nabla}W/|\vec{\nabla}W|$, the normal component of the pulse velocity, j_N, is

$$\frac{d\vec{x}}{dt} \cdot \vec{N} = -\frac{1}{|\vec{\nabla}W|} \frac{\partial W}{\partial t}. \tag{13}$$

Using Eqs. (9), $j_N = V$ and (13), we obtain the following equation for the position of the FB Γ:

$$-\frac{\partial W}{\partial t} = \frac{\pi |\vec{\nabla}W|}{4\sqrt{2[\varphi]}} \quad \text{on} \quad W(\vec{x}, t) = 0. \tag{14}$$

Thus we have posed the following FBP:

The electric potential $\varphi(\vec{x}, t)$ is a harmonic function inside and outside the FB Γ, with boundary conditions (4), (5) and (6) on the semiconductor boundaries. On the FB Γ, implicitly given by $W(\vec{x}, t) = 0$, φ has a jump discontinuity $[\varphi]$ and its normal derivative satisfies

$$(\vec{N} \cdot \vec{\nabla}\varphi)_+ = \frac{\pi}{4\sqrt{2[\varphi]}} = (\vec{N} \cdot \vec{\nabla}\varphi)_-,$$

where $\vec{N} = \vec{\nabla}W/|\vec{\nabla}W|$. Furthermore, the FB obeys the following HJE:

$$-\frac{\partial W}{\partial t} = \frac{\pi |\vec{\nabla}W|}{4\sqrt{2[\varphi]}} \quad \textit{on} \quad W = 0.$$

The conditions on the normal derivative of the electric potential at the FB are equivalent to:

$$(\vec{\nabla}\varphi \cdot \vec{\nabla}W)_+ = \frac{\pi |\vec{\nabla}W|}{4\sqrt{2[\varphi]}} = (\vec{\nabla}\varphi \cdot \vec{\nabla}W)_-$$

on $W = 0$.

The HJE (14) can be solved by the method of characteristics (the Hamilton equations). To derive them, we just take a partial derivative of the HJE with respect to x, and a partial derivative with respect to y. The results are

$$\frac{\partial}{\partial t}\frac{\partial W}{\partial x} + \frac{\pi}{4|\vec{\nabla}W|\sqrt{2[\varphi]}}\left(\frac{\partial W}{\partial x}\frac{\partial^2 W}{\partial x^2} + \frac{\partial W}{\partial y}\frac{\partial^2 W}{\partial x \partial y}\right) = \frac{\pi}{8\sqrt{2[\varphi]^3}}\frac{\partial[\varphi]}{\partial x}|\vec{\nabla}W|,$$

and a similar equation for $\partial W/\partial y$. The corresponding characteristic equations for these first-order quasilinear partial differential equations for $p = \partial W/\partial x$ and $q = \partial W/\partial y$ are

$$\begin{aligned}
\frac{dx}{dt} &= \frac{\frac{\pi}{4\sqrt{2[\varphi]}}}{\sqrt{p^2+q^2}}\,p,\\
\frac{dy}{dt} &= \frac{\frac{\pi}{4\sqrt{2[\varphi]}}}{\sqrt{p^2+q^2}}\,q,\\
\frac{dp}{dt} &= -\frac{\pi}{8\sqrt{2[\varphi]^3}}\frac{\partial[\varphi]}{\partial s}\,q,\\
\frac{dq}{dt} &= \frac{\pi}{8\sqrt{2[\varphi]^3}}\frac{\partial[\varphi]}{\partial s}\,p,\\
\frac{dW}{dt} &= 0.
\end{aligned}$$

In these equations s is arc length on the FB Γ, and we have used that $\partial[\varphi]/\partial x = -q(\partial[\varphi]/\partial s)/\sqrt{p^2+q^2}$ and $\partial[\varphi]/\partial y = p(\partial[\varphi]/\partial s)/\sqrt{p^2+q^2}$ on Γ. These expressions can be straightforwardly derived by using a local coordinate system on Γ with basis vectors $\vec{N} = \vec{\nabla}W/|\vec{\nabla}W|$ and $\vec{T} = (-\partial W/\partial y, \partial W/\partial x)/|\vec{\nabla}W|$. The jump $[\varphi]$ depends only on the arc length on Γ and t because it is defined only for $(x,y) \in \Gamma$ [these $(x,y) \in \Gamma$ have zero projection onto $\vec{N}$]. The last equation for W follows from the chain rule, the Hamilton equations for x and y and the HJE:

$$\frac{dW}{dt} = \frac{\partial W}{\partial t} + \frac{\partial W}{\partial x}\frac{dx}{dt} + \frac{\partial W}{\partial y}\frac{dy}{dt} = \frac{\partial W}{\partial t} + \frac{\pi|\vec{\nabla}W|}{4\sqrt{2[\varphi]}} = 0.$$

The characteristic equations can be used to find $W(x,y,t)$ given an initial condition $W(x_0,y_0,0) = W_0(x_0,y_0)$ such that the FB is described initially by $W_0(x_0,y_0) = 0$. Let

us assume that $[\varphi]$ is a known function of s and t. In principle, we can find the solutions of the above equations with initial data $x = x_0$, $y = y_0$, $p = \partial W_0/\partial x_0$ and $q = \partial W_0/\partial y_0$. The result is a two-parameter family of solutions $x = X(t; x_0, y_0)$, $y = Y(t; x_0, y_0)$. Let us assume that we can invert this transformation for each $t > 0$ (which should be true for t sufficiently small), $x_0 = \xi(x, y, t)$, $y_0 = \eta(x, y, t)$. The solution of the HJE is $W(x, y, t) = W_0(\xi(x, y, t), \eta(x, y, t))$ because W is constant over the characteristics. Once W is found for a given $[\varphi]$, the Laplace equation can be solved for the electric potential in the different regions of the sample separated by the FB $W = 0$. Inserting these solutions in the definition of the jump $[\varphi]$, we find an equation for this jump. It seems clear that we can implement this procedure numerically to device an explicit method such that W and $[\varphi]$ are calculated at time $t + \Delta t$ knowing their values at time t. In particular, we do not need to find (x_0, y_0) in terms of (x, y, t). All we need is to know the instantaneous location of the FB $W = 0$, thus we only need to know the evolution of those (x_0, y_0) that are on $W_0 = 0$. For each $t > 0$, the locus of such $x = X(t; x_0, y_0)$, $y = Y(t; x_0, y_0)$ constitutes the FB. More details on the numerical implementation of these ideas are given in Section V.

The FBP describes the motion of a pulse far from contacts and other boundaries or pulses. To obtain a complete asymptotic description of the Gunn self-oscillations, we have to supplement its solution with a local description of the field near the contacts and boundaries and a description of pulse collisions. In particular, new pulses are shed from the cathodes as the normal component of the current density there surpasses a critical value j_c which is the same as in the axisymmetric case [11]. There are cases in which two pulses collide and merge and cases in which a pulse splits [7]. In these cases our construction of the moving FB breaks down. What do we do then? Consider for instance two circular pulses that become tangent at a point (x_1, y_1) at time $t_1 > 0$. Clearly there are two different initial points (x_0, y_0) that have evolved towards (x_1, y_1) and $W(x, y, t)$ is no longer univalued. Numerical simulations of the complete system of equations show that the two pulses merge and adopt an eight-shaped form; see Fig. 7 of Ref. 7. To mimic this situation with our FBP, we should stop the simulations and start with a new FB at $t = t_1$ that is an eight-shaped simple curve with a hole at the tangent point of the two old pulses. The new FBP should now have a unique solution.

IV. EXACT SOLUTIONS OF THE FREE BOUNDARY PROBLEM IN SIMPLE GEOMETRIES

There are two simple geometries in which the FBP can be solved exactly: parallel planar contacts attached at the ends of a rectangular sample (1D case) and the Corbino geometry of two concentric circular contacts with the sample in between (axisymmetric case). Let us call region A that comprising the cathode and region B that comprising the anode.

A. 1D geometry

Then the electric potential depends only on the coordinate x, the cathode is located at $x = 0$, the anode at $x = L$ and the FB is a moving point $x_s(t)$. The electric potential obeys

$$\frac{\partial^2 \varphi_A}{\partial x^2} = 0 \text{ in } (0, x_s),\ \varphi_A(0,t) = 0, \frac{\partial \varphi_A}{\partial x}(x_s,t) = \frac{\pi}{4\sqrt{2[\varphi]}};$$
$$\frac{\partial^2 \varphi_B}{\partial x^2} = 0 \text{ in } (x_s, L),\ \varphi_B(L,t) = \Phi, \frac{\partial \varphi_B}{\partial x}(x_s,t) = \frac{\pi}{4\sqrt{2[\varphi]}}.$$

The solutions are

$$\varphi_A(x,t) = \frac{\pi}{4\sqrt{2[\varphi]}}\, x,$$
$$\varphi_B(x,t) = \frac{\pi}{4\sqrt{2[\varphi]}}\, (x - L) + \Phi.$$

The jump in the potential, $[\varphi] = \varphi_B(x_s,t) - \varphi_A(x_s,t)$ is independent of t and x_s, and it solves the following equation:

$$[\varphi] = \Phi - \frac{\pi}{4\sqrt{2[\varphi]}}\, L.$$

Setting $\alpha = \sqrt{[\varphi]}$ and $\phi = \Phi/L$, we obtain

$$\alpha^3 = \left(\phi\, \alpha - \frac{\pi}{4\sqrt{2}}\right) L. \tag{15}$$

Depending on the values of ϕ and L this equation may have zero, one or two positive solutions. If there are two solutions, an argument due to Volkov and Kogan [14] shows that the pulse with smaller $[\varphi]$ is unstable. The FB $x_s(t)$ can be found by solving the dynamical

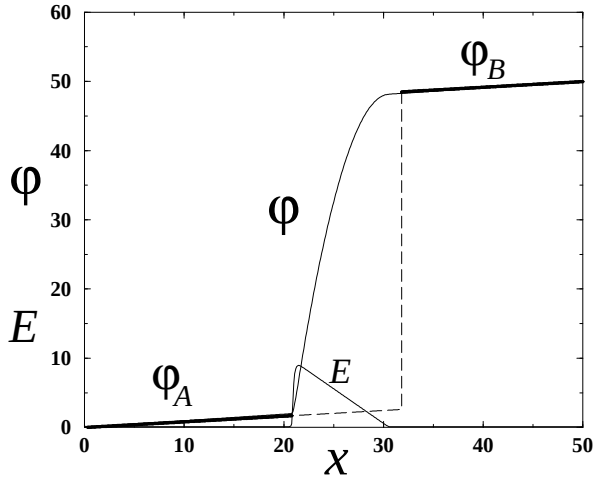

FIG. 1: The solid lines indicate the electric potential and field of an advancing 1D pulse (far from the contacts) calculated by numerically solving the Kroemer model. They agree very well with the approximations $\varphi_A(x,t)$ and $\varphi_B(x,t)$ (dashed lines). We have used the nondimensional units defined in the text.

HJE:

$$-\frac{\partial W}{\partial t} = \frac{\pi}{4\sqrt{2[\varphi]}} \left| \frac{\partial W}{\partial x} \right| .$$

Let us assume that the initial profile $W(x,0) = W_0(x)$ is monotone increasing and that it vanishes at a position $x_s(0) \in (0,L)$ corresponding to the pulse location at time $t = 0$. For small enough t, we then have $\partial W/\partial x > 0$ and we can ignore the absolute value in the previous equation. Its solution is then

$$W(x,t) = W_0 \left(x - \frac{\pi t}{4\sqrt{2[\varphi]}} \right) .$$

Notice that we have $\partial W/\partial x > 0$ for all $t > 0$. Since $W(x_s,t) = 0$, the previous solution yields

$$x_s(t) = x_s(0) + \frac{\pi}{4\sqrt{2[\varphi]}}\, t. \tag{16}$$

Fig. 1 compares $\varphi_A(x,t)$ and $\varphi_B(x,t)$ to the electric potential of an advancing pulse calculated by numerically solving the exact system of equations.

The FBP has yielded the same approximation to the complete 1D problem as indicated in Ref. 9 for the motion of a pulse far from the boundaries. When the pulse arrives at the

anode $x = L$, it starts disappearing there and the current density increases until it surpasses j_c. Then a new pulse is shed at $x = 0$; see Ref. 9 for details.

B. Corbino geometry (axisymmetric case)

The potential depends only on the radius r measured from the center of the cathode. Solving the Laplace equation $\partial[r\,\partial\varphi/\partial r]/\partial r = 0$ at both sides of the moving pulse of radius $r_s(t)$, we find

$$\begin{aligned} \varphi_A(r,t) &= \frac{\pi\, r_s}{4\sqrt{2[\varphi]}}\, \log\left(\frac{r}{r_c}\right), \\ \varphi_B(r,t) &= \frac{\pi\, r_s}{4\sqrt{2[\varphi]}}\, \log\left(\frac{r}{r_c+L}\right) + \Phi. \end{aligned}$$

The jump in the electric potential at r_s is now given by the following equation:

$$[\varphi] = \Phi - \frac{\pi\, r_s}{4\sqrt{2[\varphi]}}\, \log\left(\frac{r_c+L}{r_c}\right),$$

or equivalently

$$\alpha^3 = \Phi\,\alpha - \frac{\pi}{4\sqrt{2}}\, \log\left(\frac{r_c+L}{r_c}\right)\, r_s. \tag{17}$$

for $\alpha = \sqrt{[\varphi]}$. Notice that r_s explicitly appears in these equations and that $[\varphi]$ decreases as the pulse advances (and therefore r_s increases); cf. Ref. 11. The HJE can be solved as in the 1D case and its solution yields

$$r_s(t) = r_s(0) + \frac{\pi}{4\sqrt{2}} \int_0^t [\varphi]^{-\frac{1}{2}}\, dt. \tag{18}$$

In this case, Eqs. (17) and (18) for $[\varphi]$ and $r_s(t)$ need to be solved simultaneously.

The stage of a self-oscillation described by the previous FBP corresponds to having a single pulse far from the contacts. See Ref. 11 for a fuller description of self-oscillations in this case.

V. NUMERICAL RESULTS

To test our FBP formulation, we shall consider the relatively complicated geometry of Fig. 7 in Ref. 7 (reproduced here as Fig. 2 to facilitate comparison with the results of

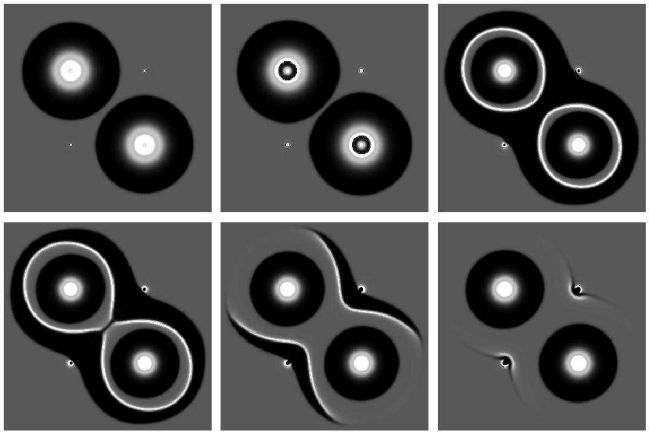

FIG. 2: Density plots of the solution of the Kroemer's model (with $v_s = 0$) in a square of side l=20 with four circular contacts forming the vertices of a square of side $d = 4$ located at the center of the sample. Cathodes have potential $\varphi = 0$ and anodes have $\varphi = 10$. Our dimensionless units have been defined in Section II.

numerically solving the FBP) corresponding to $v_s = 0$. The sample is a square of side $l = 20$ with two cathodes at potential $\varphi = 0$ and two anodes with $\varphi = 10$. The circular contacts (of radii 0.5) are at the vertices of a square of side $d = 4$ located at the center of the sample. Then the separation between contacts is $L = 3$ and the distance from contacts to the border of the sample is 7.5. Notice that dipole waves are emitted from the cathodes. Immediately after their emission, the waves are circular. As they approach each other, the waves become elongated and merge forming an eight-shaped connected curve that grows until it reaches the anodes.

A. Free boundary problem

We shall now explain the results obtained by solving numerically the FBP. Details of the numerical method will be given later. Fig. 3 shows the evolution of the FB separating the two regions of the sample, inside and outside the boundary. Notice that the numerical solution of the FBP closely resembles the numerical solution of the full Kroemer model depicted in Fig. 2. In the two first frames of Fig. 3, the FB consists of two circumferences corresponding to the dipole waves nucleated at the cathodes. In the third frame, the curves collide and then merge forming an eight-shaped closed curve as shown in the remaining

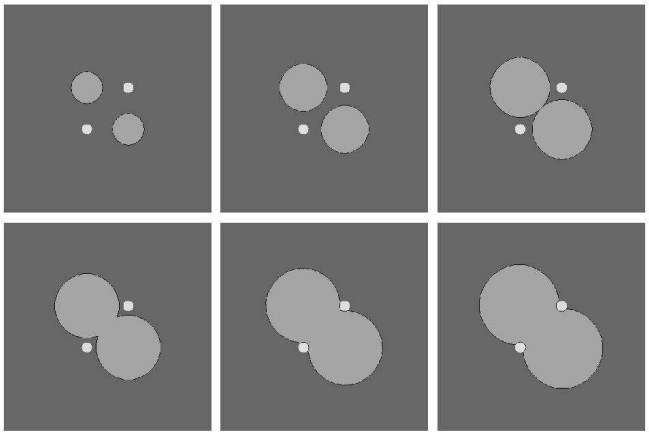

FIG. 3: Time evolution of the FB (black curve) separating the two regions of the sample, inside (clear grey) and outside (dark grey) the boundary. The anodes appear in white.

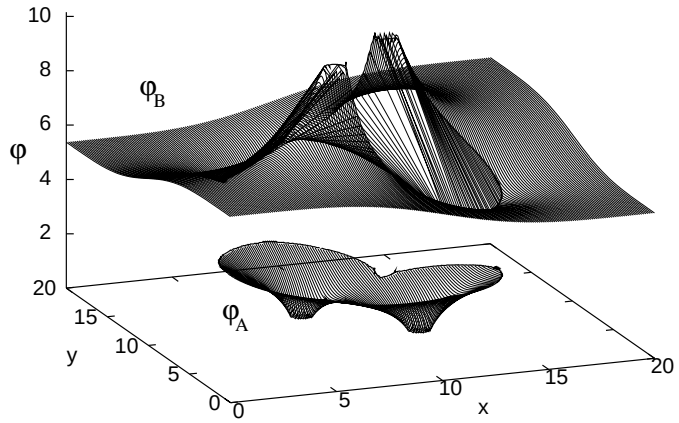

FIG. 4: 3D plot of the electric potential surfaces $\varphi_A(x, y, t)$ (lower surface, inside the FB) and $\varphi_B(x, y, t)$ (upper surface, outside the FB) at the time corresponding to the last frame of Fig. 3. Our dimensionless units have been defined in Section II.

frames of Fig. 3. Fig. 4 shows the electric potential distribution in each region (inside and outside the FB) corresponding to the last frame of Fig. 3.

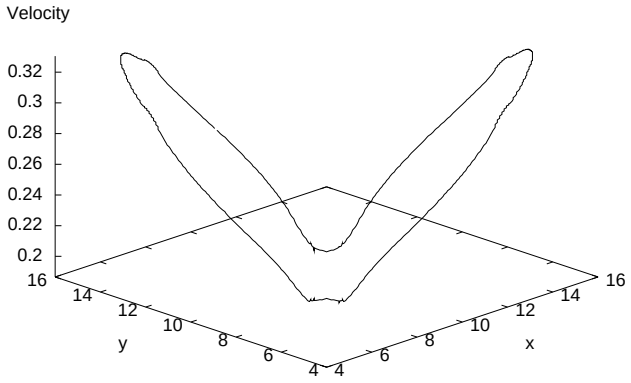

FIG. 5: Dimensionless velocity of each point of the FB at the dimensionless time corresponding to the last frame in Fig. 3 and calculated from the electric potential distribution showed in Fig. 4.

By using Eq. (9) we see that each point of the FB moves with velocity

$$V = \frac{\pi}{4\sqrt{2[\varphi]}}.$$

Fig. 5 depicts the velocity of the points at the FB in the last frame of Fig. 3. The curve is symmetric and Fig. 5 shows that the FB moves faster at the points located in the left-upper and right-lower corners of the sample, in agreement with the numerical solution of the Kroemer model.

Let t_1 be the time at which two dipole waves created at the cathodes touch at a point (as in the third frame of Fig. 3), counted from the time at which dipole waves are emitted at the cathodes ($t = 0$). The velocity of the points at the FB is shown at three different times in Figures 6 ($0 < t < t_1$) and 7 ($t > t_1$). Notice that the velocity of the points near the center of the sample in Fig. 6 is larger than in neighboring points, which explains the elongated form of the dipole waves in the numerical solution of the Kroemer model (see the third and fourth images of Fig. 2). In Fig. 7 we observe that the largest velocity is reached at the outer points of the single FB, also in agreement with the numerical solution of the full model equations.

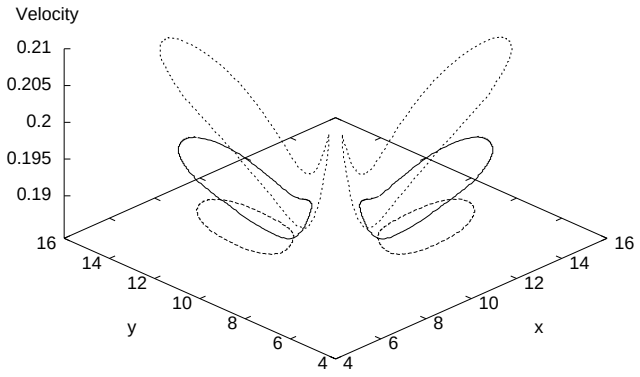

FIG. 6: Time evolution (from bottom to top) of the velocity of the FB Γ when $t < t_1$, where the topology is composed by three domains and Γ is made of two circumferences. Our dimensionless units have been defined in Section II.

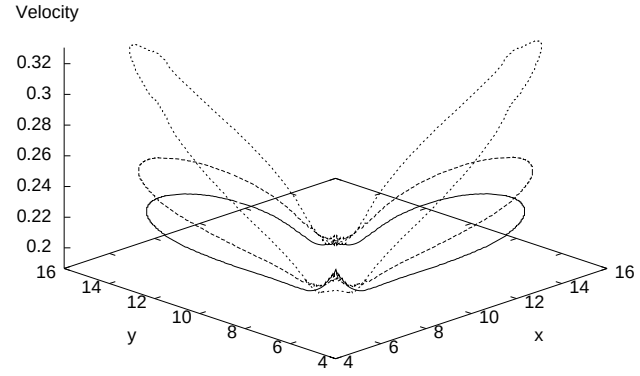

FIG. 7: Time evolution (from bottom to top) of the velocity of the FB Γ when $t > t_1$. The topology is now composed by two domains.

B. Numerical solution of the free boundary problem

To solve numerically the FBP, we should solve the PDE governing the time evolution of the FB, taking into account that the velocity thereof is determined by the solution of Laplace's equation with Neumann boundary conditions on the FB and Dirichlet boundary

conditions at the contacts (the electric potential problem, or, briefly, the EPP).

At each time step, the FB advances at a constant velocity for a short distance from its previous position. (Thus we ignore the velocity variation during the short time interval between t_i and $t_i + \Delta t$). At time $t_i + \Delta t$, we solve the EPP in the different domains resulting from the new location of the FB. This yields the electric potential distribution that is used to calculate the velocity of the FB at the next time step.

The time evolution of the free boundary is calculated by using the so-called fast marching method (a special case of the method of level sets). This method was introduced by Sethian in 1996 [15] and used in a wide variety of applications [16, 17, 18]. Level sets methods are very efficient for solving complex problems of evolving interfaces whose topology may change. If the velocity of the interface does not change sign, the fast marching method is a very fast algorithm indeed.

The general version of the method of level sets consists of solving the evolution equation

$$\frac{\partial W}{\partial t} + F|\vec{\nabla} W| = 0, \tag{19}$$

where $W(\vec{x}, t)$ is a function such that $W{=}0$ describes the free boundary moving at velocity F; cf. Eq. (14). When the sign of F does not change, the FB either expands or contracts uniformly as time elapses. In our case, the FB moves away from the cathodes. Then the zero-level set $W{=}0$ comprises the points farthest from the cathodes that have been traversed once by the FB at a given instant of time. Then we can define an *arrival time* function T in the whole sample: $T(\vec{x})$ is the time it takes the FB to arrive at the point $\vec{x}$ starting from a given initial configuration. To find an equation for T, we take the gradient of $W(\vec{x}, T(\vec{x})) = 0$, $\vec{\nabla} W + W_t \, \vec{\nabla} T = 0$, and use Eq. (19) to obtain

$$\vec{\nabla} W - F|\vec{\nabla} W| \, \vec{\nabla} T = 0. \tag{20}$$

This equation implies that $\vec{\nabla} W$ and $\vec{\nabla} T$ are colinear vectors and their lengths are related by $|\vec{\nabla} W| = F|\vec{\nabla} W| \, |\vec{\nabla} T|$. Then we obtain the following Eikonal equation for T,

$$|\vec{\nabla} T(\vec{x})| = \frac{1}{F(\vec{x})} \equiv \frac{4\sqrt{2\,[\varphi]}}{\pi}. \tag{21}$$

The velocity F as a function of $\vec{x}$ is evaluated at time t. Once the solution of Eq. (21) is known at a narrow band about the instantaneous location of the FB at time t, the location thereof at time $t + \Delta t$ is found by solving $T(\vec{x}) = t + \Delta t$.

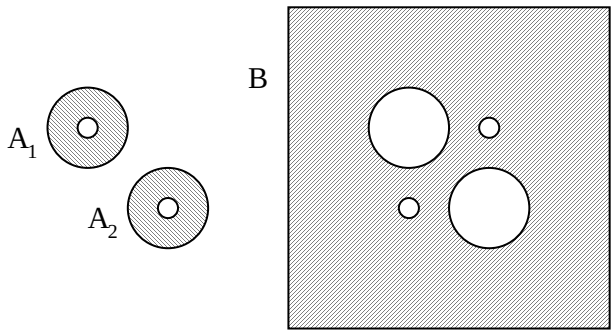

FIG. 8: The FB comprises two separate curves defining three regions.

The fast marching method consists of solving numerically this equation by using upwind finite differences to approximate $|\vec{\nabla}T|$. In particular, we have used the Godunov scheme

$$\max\left(\frac{T_{i,j}-T_{i-1,j}}{\Delta x},\frac{T_{i,j}-T_{i+1,j}}{\Delta x},0\right)^2+ \max\left(\frac{T_{i,j}-T_{i,j-1}}{\Delta y},\frac{T_{i,j}-T_{i,j+1}}{\Delta y},0\right)^2=\frac{1}{F_{i,j}^2}. \tag{22}$$

This choice ensures that the information is always taken from where the solution is already known. The fast marching method is consistent with the Huygens principle even when two waves collide and adopt an eight-shaped curve as in Fig. 2, or with even more complex topologies. The EPP is solved by using an integral equation method based upon Green's formula. This yields the solution φ within a region for a given value of its normal derivative at each point of the boundary. To make sure that the nonlinear boundary conditions at the FB hold, we implement an iterative process.

We shall start our simulation from an initial configuration as depicted in Fig. 8. There two waves have been nucleated at the cathodes and have reached their typical circular form. The FB consists of two circumferences that divide the sample in three regions, A_1, A_2 and B, in which we should simultaneously solve the EPP. Implementing the fast marching method, we see two waves growing from the initial circumferences until a time t_1, when they meet at the center of the sample. Then the FB is a connected curve and we have the situation depicted in Fig. 9, where there are only two regions A and B. The algorithm detects the time t_1, adapts itself immediately to the new configuration similar to Fig. 9 and it continues solving the FBP.

The accuracy and convergence of the method have been successfully checked by decreas-

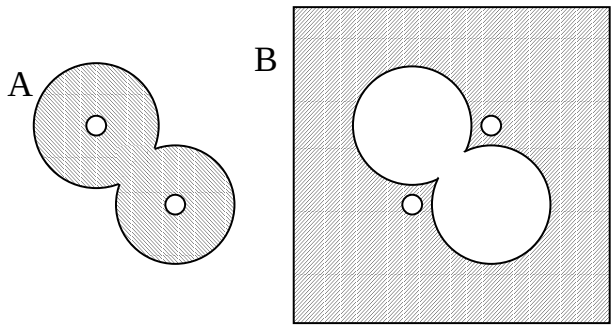

FIG. 9: The FB is a single curve defining two regions.

ing the mesh size. The computational cost of the method is very low compared to the computational and memory effort required by the resolution of the full Kroemer model. The order-one fast marching method solves the Eikonal equation in the whole sample with $O(N \log N)$ operations, where N is the size of the mesh, but we only need to solve the Eikonal equation in a narrow band ahead of the FB at each time step. On the other hand, the EPP solver carries out $O(N^2 + M)$ operations, where M is the number of points defining the FB (at most of order N).

VI. CONCLUSIONS

We have studied Gunn oscillations in 2D rectangular samples of n-GaAs with circular contacts by solving the Kroemer drift-diffusion model with appropriate boundary and initial conditions. By using singular perturbation methods, the motion of dipole waves in semiconductor samples has been reduced to solving a free boundary problem. Exact solutions of this problem have been found in simple 1D and axisymmetrical (Corbino) geometries. In the general case, the free boundary is numerically found by means of the fast marching method which is a special case of the method of level sets. The great reduction in computational cost allowed by using this method as an alternative to solving the full Kroemer model would enable us to study much larger samples.

Acknowledgments

This work has been supported by the Spanish MCyT through grant BFM2002-04127-C02-01, by the Third Regional Research Program of the Autonomous Region of Madrid (Strategic Groups Action), and by the European Union under grant HPRN-CT-2002-00282. We thank G. Oleaga for fruitful discussions.

---

[*] E-mail: `bonilla@ing.uc3m.es`

[†] E-mail: `escobedo@math.uc3m.es`

[‡] E-mail: `higuera@dmt.upm.es`

[1] J. D. Murray, *Mathematical Biology*, 2nd ed. (Springer, Berlin, 1993).

[2] J.P. Keener and J. Sneyd, *Mathematical Physiology*, (Springer, New York, 1998).

[3] Y. Kuramoto, *Chemical Oscillations, Waves, and Turbulence*, (Springer, Berlin, 1984).

[4] F.-J. Niedernostheide, editor, *Nonlinear Dynamics and Pattern Formation in Semiconductors and Devices*, Vol. 79 of *Springer Proceedings in Physics*, (Springer-Verlag, Berlin-Heidelberg, 1995).

[5] J. B. Gunn, Solid-State Comm. **1**, 1 (1963).

[6] B. Willing and J. C. Maan, Phys. Rev. B **49**, 13995 (1994). B. Willing, Ph.D. Thesis, University of Nijmegen, 1994.

[7] L. L. Bonilla and R. Escobedo, Phys. Rev. E **64**, 036203 (2001).

[8] R. Escobedo, Ph.D. Thesis, Universidad Carlos III de Madrid, 2001.

[9] F. J. Higuera and L. L. Bonilla, Physica D **57**, 161 (1992).

[10] L. L. Bonilla, I. R. Cantalapiedra, G. Gomila and J. M. Rubí, Phys. Rev. E **56**, 1500 (1997).

[11] L. L. Bonilla, R. Escobedo and F. J. Higuera, Phys. Rev. E **65**, 016607 (2001).

[12] H. Kroemer, IEEE Trans. Electron Devices **ED-13**, 27 (1966).

[13] Outside the pulse, the field is quasistationary, so that $E_- \approx E_1(j_N)$.

[14] A. F. Volkov and Sh. M. Kogan, Sov. Phys. Usp. **11**, 881 (1969). [Usp. Fiz. Nauk. **96**, 633 (1968)].

[15] J. A. Sethian, Proc. Natl. Acad. Sci. USA **93**, 1591 (1996).

[16] J. A. Sethian, SIAM Rev. **41**, 199 (1999).

[17] D. L. Chopp, SIAM J. Sci. Comput. **23**, 230 (2001).

[18] D Adalsteinsson and J. A. Sethian, J. Comp. Phys. **148**, 2 (1999).